






Article

Enhancement of Optical Telecommunication Bands: Pr³⁺-Doped Halide Phosphate Glasses Display Broadband NIR Photoluminescence Emission

Bilel Charfi ¹, Kamel Damak ¹, Ramzi Maâlej ¹, Mohammed S. Alqahtani ^{2,3}, Khalid I. Hussein ^{2,4}, Ali M. Alshehri ⁵, Abdulrahman M. Hussain ², Bozena Burtan-Gwizdala ⁶, Manuela Reben ⁷, and El Sayed Yousef ^{5,8,*}

¹ LaMaCoP, Faculty of Sciences of Sfax, University of Sfax, Sfax 3018, Tunisia

² Department of Radiological Sciences, College of Applied Medical Sciences, King Khalid University, Abha 61421, Saudi Arabia

³ BioImaging Unit, Space Research Centre, Department of Physics and Astronomy, University of Leicester, Leicester LE1 7RH, UK

⁴ Department of Medical Physics and Instrumentation, National Cancer Institute, University of Gezira, Wad Medani 2667, Sudan

⁵ Physics Department, Faculty of Science, King Khalid University, Abha 61413, Saudi Arabia

⁶ Institute of Physics, Cracow University of Technology, ul. Podchorazych 1, 30-084 Cracow, Poland

⁷ Faculty of Materials Science and Ceramics, AGH–University of Science and Technology, al. Mickiewicza 30, 30-059 Cracow, Poland

⁸ Research Center for Advanced Materials Science (RCAMS), King Khalid University, Abha 61413, Saudi Arabia

* Correspondence: ayousf@kku.edu.sa



Citation: Charfi, B.; Damak, K.; Maâlej, R.; Alqahtani, M.S.; Hussein, K.I.; Alshehri, A.M.; Hussain, A.M.; Burtan-Gwizdala, B.; Reben, M.; Yousef, E.S. Enhancement of Optical Telecommunication Bands: Pr³⁺-Doped Halide Phosphate Glasses Display Broadband NIR Photoluminescence Emission. *Materials* **2022**, *15*, 6518. <https://doi.org/10.3390/ma15196518>

Academic Editors: Laetia Petit and Arnaud Lemiere

Received: 5 August 2022

Accepted: 16 September 2022

Published: 20 September 2022

Publisher's Note: MDPI stays neutral with regard to jurisdictional claims in published maps and institutional affiliations.



Copyright: © 2022 by the authors. Licensee MDPI, Basel, Switzerland. This article is an open access article distributed under the terms and conditions of the Creative Commons Attribution (CC BY) license (<https://creativecommons.org/licenses/by/4.0/>).

Abstract: In the optical energy gap, visible and near-IR emission of halide phosphate glasses with a composition of 40P₂O₅-30ZnO-20LiCl-10BaF₂ in mol% doped with 3.5 × 10⁴ ppm Pr₂O₃, referred to as PZLBPr, were synthesized. The UV-VIS-NIR and spectroscopic properties of these glasses were also predicted. The current glasses had broadband emission photoluminescence covering a wavelength range of 1250 to 1700 nm when excited at 455 nm. These bands for near-infrared emission luminescence relate to the transitions ¹G₄ → ³H₅, ¹D₂ → ¹G₄, and ³H₄ → ³F₃, ³F₄ in the optical telecommunication window. The significant PL emission wideband was caused by the radiative transition from Pr³⁺: ¹D₂ to ¹G₄. At 445 nm excitation, these glasses exhibited emission bands that corresponded to blue/reddish orange spectral ranges in visible ranges. The prepared glass has a high lasing quality factor ($\Omega_4/\Omega_6 = 0.9$), high optical energy (4.72 eV), and quantum efficiency = 87.3% with FWHM = 156 nm of transition emission from the ¹D₂ → ¹G₄ level. As a result, broadband near infrared optical amplifiers can be fabricated from the prepared glasses.

Keywords: phosphate glasses; rare earth; spectroscopic; Judd–Ofelt; photoluminescence

1. Introduction

The C-, S-, E-, and O bands may be enhanced with the use of rare earth RE ions including Er³⁺, Tm³⁺, and Ho³⁺ [1–5]. It has been investigated whether the co-doped RE ions may improve population inversion and increase bandwidth [2,3] to avoid a number of undesirable parameters, such as frequent cross-relaxation and concentration quenching occurring. In order to overcome the restrictions of the RE ion multi-doped system, an efficient RE ion single-doped ultra-broadband signal amplification medium must be developed. The commercial Er³⁺-doped fiber amplifiers (EDFA) based on silicate glass have low linewidths, which reduce NIR transmission [5–8].

In consideration of this, new glass host matrices containing rare earths with extended lifetimes for signal amplification in optical telecommunications must be searched for. Pr³⁺, a trivalent rare earth ion, displays broad near-infrared luminescence as a result, which is

required for optical fiber amplifiers that operate in the O-, E-, S-, C-, and L-bands [1,2] in the 1.2 to 1.7 μm wavelength range of 1.2 to 1.7 μm .

Studies in the past have shown the optical amplification potential of Pr^{3+} ions existing in a variety of inorganic glasses, particularly those with low-loss NIR transmission windows [3,8]. Low-loss NIR luminescence in the $^1\text{D}_2 \rightarrow ^1\text{G}_4$ transition of Pr^{3+} transition correlates to super broadband NIR luminescence.

In heavy metal oxide glasses, the luminescence spectroscopy of Pr^{3+} ions was studied in [9–13]. As a result of energy transfer from Pr^{3+} to Yb^{3+} ions, we recently described the intense NIR emission at 1000 nm with a down-conversion mechanism under excitation of 445 nm [14]. The down-conversion processes in $\text{Pr}^{3+}/\text{Yb}^{3+}$ co-doped devices that convert a blue photon into two NIR photons have also been reported. Trivalent Yb^{3+} emission at 1000 nm may be captured by silicon solar cells without any losses (1.05 eV) because its single $^2\text{F}_{5/2}$ excited state is close to the silicon band gap [15].

Fiber lasers and optical amplifiers have revealed the phosphate glasses to be an excellent product because of their superior thermal stability, flexibility, and mechanical strength [6,7,16]. For the first time, near-IR luminescence has been seen in $40\text{P}_2\text{O}_5\text{-}30\text{ZnO-}20\text{LiCl-}10\text{BaF}_2$ glasses with single doped 3.5×10^4 ppm of Pr^{3+} , which we describe in this paper. As an additional factor, the Pr^{3+} ligand field was modified by the addition of certain halides (F^- and Cl^-). Moreover, we estimated the spectroscopic parameters viz. branching ratio, radiative lifetime, spontaneous emission probability, and quantum efficiency of the $^1\text{D}_2$ level of Pr^{3+} . The results show that the produced glass may be used to create broadband fiber amplifiers that operate in optical communications.

2. Experimental Work

Glass composed of $40\text{P}_2\text{O}_5\text{-}30\text{ZnO-}20\text{LiCl-}10\text{BaF}_2$ in mol% doped with 3.5×10^4 ppm Pr_2O_3 is referred to as (PZLBPr), which has a high homogeneity. Following the melt quenching method, we used a muffle furnace to melt the chemical at 1150 °C for one hour after stirring it in a platinum crucible. A copper mold was then used to cast the molten chemical combination. The annealing procedure started with a 2 h heat treatment of the quenched glass at 440 °C to remove any strain from the produced glasses. To investigate the amorphous characteristics of produced glasses, the powder X-ray diffraction pattern (XRD-Philips PW (1140) diffractometer and copper target ($K = 1.54$)) were used.

A gas pycnometer was used to determine the density of the glass (Model: UltraPyc 1200 e). The density of the PZLBPr glass sample was measured to be 3.837 ± 0.00015 g/cm³. The optical absorption spectra of the glasses were determined in the wavelength range of 190–2500 nm using a UV-VIS-NIR spectrophotometer (JASCO, V-570). The short pulse stimulation was carried out using an optical parametric oscillator operated by a third harmonic of a Nd:YAG laser, and the luminescence decay curves were obtained as a result. Using an Optron Dong Woo fluorometer system, the photoluminescence spectra were measured [17].

The following equation may be used to determine the Pr^{3+} ions concentration [13]:

$$N_{\text{Pr}^{3+}} = 2 \frac{3.5\rho A_v}{100M} \quad (1)$$

where M is the PZLBPr glass's molecular weight and A_v is the Avogadro's number. In this PZLBPr glass, the dopant Pr^{3+} concentration is $N_{\text{Pr}^{3+}} = 1.3628 \times 10^{27}$ ions/m³.

3. Results and Discussion

To determine whether the produced glasses are amorphous or crystalline, XRD analysis was performed. Figure 1 displays the XRD patterns of the samples of prepared glasses. The X-ray amorphous patterns can be observed in the data, and because the indicated crystalline phase had not developed the amorphous nature was anticipated. According to the photo of prepared glasses PZLBPr in Figure 2b, they were transparent and homogenous. According to Figure 2a, the PZLBPr sample's UV-Vis-NIR absorption spectrum exhibits peaks at

wavelengths around 444, 466, 476, 590, 1014, 1538, 1942, and 2354 nm that correspond to transitions from the ground state of 3H_4 to excited states of 3P_2 , 3P_1 , 3P_0 , 1D_2 , 1G_4 , 3F_4 , 3F_3 , 3F_2 , and 3H_2 , respectively. The transition from 3H_4 to 3F_3 has the highest peak, whereas the transfer from 3H_4 to 1G_4 has the lowest peak. The occurrence of all these peaks is in agreement with findings regarding other glasses doped with Pr^{3+} [18–22].

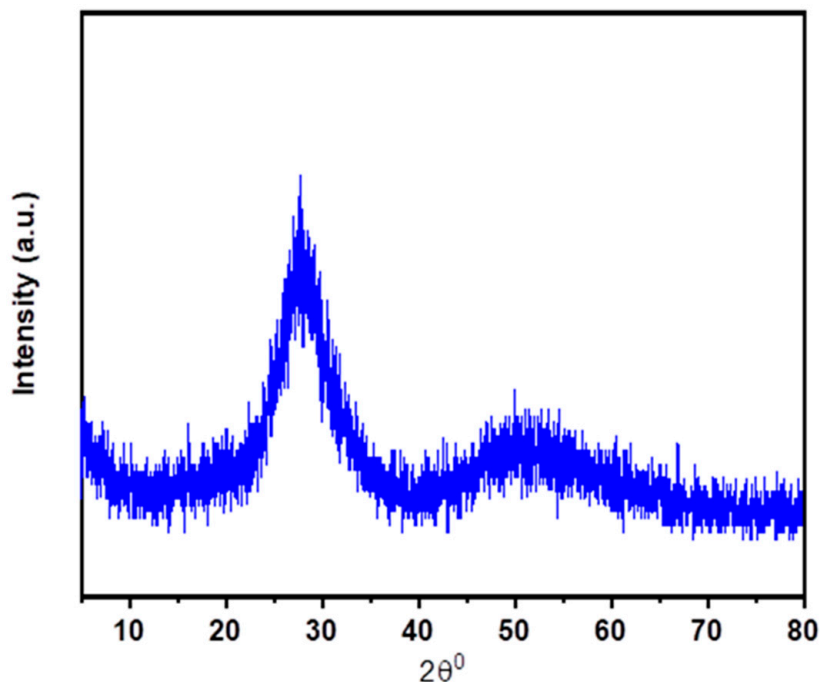


Figure 1. XRD profile of prepared glasses.

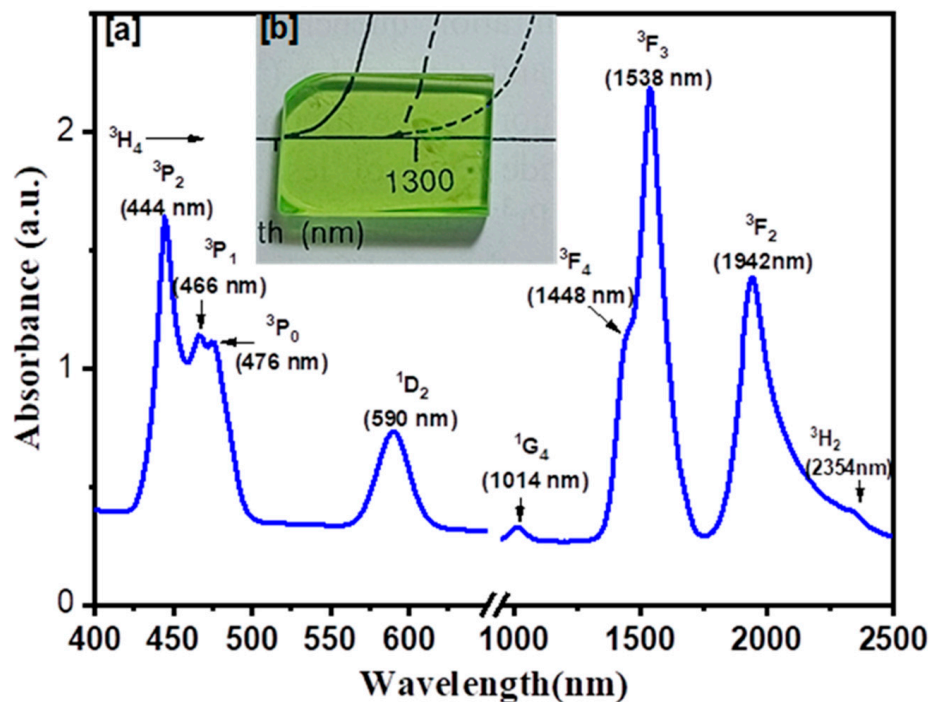


Figure 2. (a) PZLBPr glass absorption spectra, with each peak’s transition state specified; (b) photograph of the prepared glasses after annealing.

The value of optical energy gap, E_{opt} , is calculated using the basic relation established for amorphous materials by Mott and Davis [23] based on the absorption coefficient (α) and the photon energy ($h\nu$) as follows:

$$(\alpha h\nu) = C(h\nu - E_{opt})^m \quad (2)$$

where m changes based on the interband transition process and C is a constant. As shown in Figure 3, the best fit to the observed data showed that $m = 2$ indicated the indirect allowed transition in the gap of the prepared glass, which means that it is a suitable method for the prediction of the optical energy gap and optical properties of glass materials.

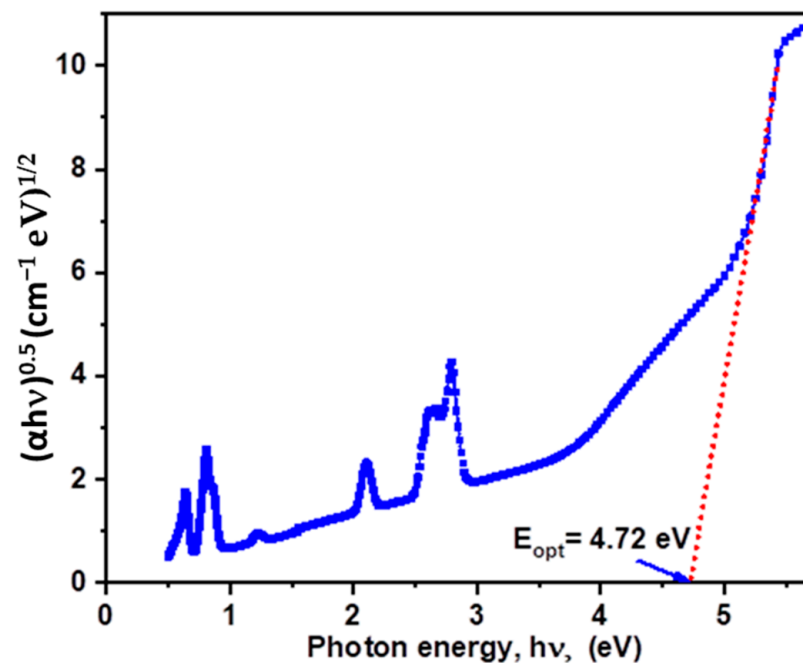


Figure 3. Relation between $(h\alpha\nu)^{0.5}$ vs. $h\nu$ of PZLBPr glasses.

The indirect transitions allowed in inorganic glasses are represented by a straight line at $(\alpha h\nu)^{1/2} = 0$, with an $h\nu$ axis in Equation (2), which illustrates the prepared glasses (see Figure 3). The results obtained showed that the value of E_{opt} is 4.72 ± 0.01 eV for PZBLPr glass. It has the highest value of E_{opt} compared to tellurite glass and other glass doped with the $\text{Nd}^{3+}/\text{Yb}^{3+}$ system that have been reported previously [24–27]. This is due to the presence of Pr^{3+} ions, which leads to an increase in both the width of the localized state in the forbidden gap and the density of electrons, therefore, increasing the probability of electronic transition from the valence band to the conduction band.

The incorporation (F, Cl) improved the phosphate glass matrix by increasing the solubility of rare earth, which means that the glass network can form more than one electric dipole environment for rare-earth ions. Consequently, the fluorescence line shape and radiative and non-radiative rates may be created in hybrid glass structures. Furthermore, the F and Cl ions in the prepared glass reduce the OH^- and Pr^{3+} ions, which enter the lattice sites by replacing OH ions. Furthermore, the halide ions F^- and Cl^- can lead to an increase in the ionicity and consequently decrease the covalency of the network structure of matrix glasses, which results in a larger optical energy gap when compared to oxide phosphate glasses reported in the literature [28–30]. This can be considered an advantage because the wide band gap of this glass can form an excellent medium with doping or co-doped rare earth to produce superior materials that can be used in optical telecommunication at ultrabroad NIR.

Here, we determine the Urbach energy, E_{Ub} , using the relationship between the photon energy ($h\nu$) and optical absorption coefficients in glasses established by [23].

$$\alpha(\nu) = A \exp\left(\frac{h\nu}{E_{Ub}}\right) \quad (3)$$

where A is a constant and E_{Ub} is the Urbach energy corresponding to the extent of the tail of localized states in the band gap. The phonon-assisted indirect electronic transitions are responsible for E_{Ub} . The reciprocals of the slopes of the linear component of the $\ln(\alpha)$ vis. $h\nu$ curves in the lower photon energy areas were used to calculate the E_{Ub} value (0.07 eV) (see Figure 4).

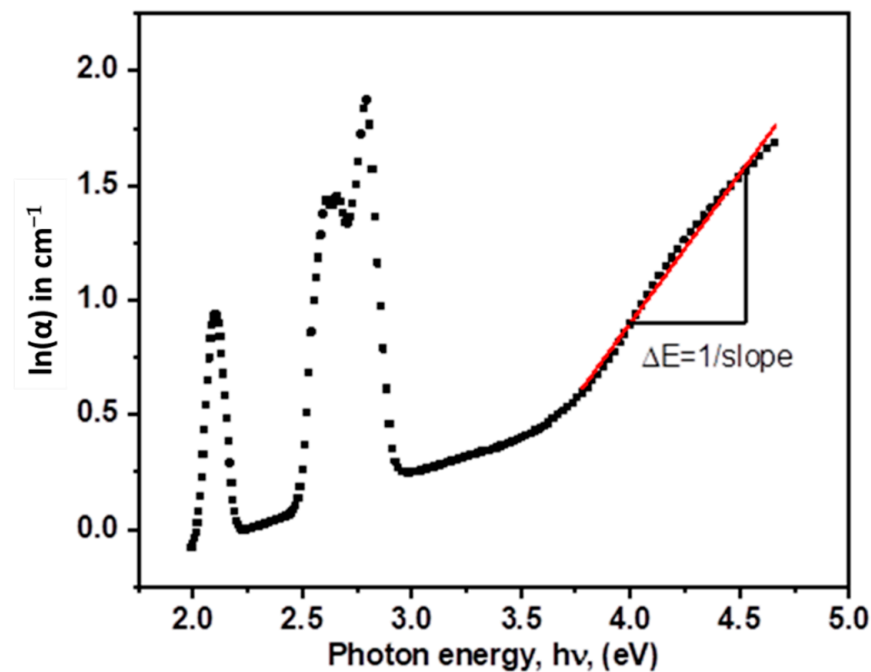


Figure 4. The relation between $\ln(\alpha)$ vis. $h\nu$ of PZLBPr glasses.

The Judd–Ofelt (JO) analysis was used to calculate the spectroscopic characteristics of this glass system using the absorption intensities of Pr^{3+} -doped PZLBPr. A basic description of the JO analysis is provided here. The literature [31–33] includes all the applications of the JO model.

The formula below yields the measured line strength $S_{\text{exp}}(J \rightarrow J')$ of a particular band:

$$S_{\text{exp}}(J \rightarrow J') = \frac{9n}{(n^2 + 2)^2} \cdot 4\pi\epsilon_0 \cdot \frac{3c \cdot h \cdot (2J + 1)}{8\pi^3 e^2} \cdot \frac{2.303}{N \cdot l \cdot \lambda} \cdot \Gamma - n \cdot S_{md}(J \rightarrow J') \quad (4)$$

where l is the studied sample's thickness (6.22 mm), c is the speed of light, h is Planck's constant, e is the elementary charge, J is the angular momentum of the initial state, N is the density of ions, λ is the mean wavelength of the absorption bands, and $\Gamma = \int OD(\lambda) \cdot d\lambda$ is the experimental integrated optical density in the wavelength range. This density can be determined by calculating the total area under the absorbed band.

For many transitions of the Pr^{3+} ion, the contribution of the magnetic dipole, S_{md} , to the observed line strength is generally small [19,22,34,35]. Because of this, the magnetic-dipole contribution was neglected in the prepared glasses. Table 1 depicts the results of the line-strength calculations and intensity measurements for the selected transitions.

Table 1. The results of the line-strength calculations and intensity measurements for the transitions performed.

	λ (nm)	ν (cm ⁻¹)	$ U^2 ^2$	$ U^4 ^2$	$ U^6 ^2$	Γ (nm·cm ⁻¹)	S_{exp} (10 ⁻²⁴ m ²)	S_{cal} (10 ⁻²⁴ m ²)
³ H ₄ → ³ P ₂	445	22471	0	0.0362	0.1355	19.11	0.54705	0.30554
³ P ₁	462	21652	0	0.1707	0	7.51	0.20720	0.28026
³ P ₀	476	21012	0	0.1728	0	14.61	0.39129	0.28371
¹ D ₂	590	16956	0.0026	0.017	0.052	10.31	0.22271	0.12241
³ F ₃	1541	6490	0.0654	0.3469	0.6983	215.68	1.78360	1.83910
³ F ₂	1958	5106	0.5089	0.4032	0.1177	137.06	0.89182	0.88521

On the other hand, in the Judd–Ofelt theory, the line strength $S_{\text{cal}}(J \rightarrow J')$ between the initial state J characterized by (S, L, J) and the final state J' given by (S', L', J') can be calculated using the following expression [31–33].

$$S_{\text{cal}}(J \rightarrow J') = \sum_{t=2,4,6} \Omega_t \left| \langle SLJ || U^{(t)} || S'L'J' \rangle \right|^2 \quad (5)$$

where Ω_t ($t = 2, 4, 6$) denotes the doubly reduced matrix elements and t represents the Judd–Ofelt parameters. $||U^{(t)}||^2$ ($t = 2, 4, 6$) represent the reduced matrix elements utilized for the absorption transitions of this Pr³⁺-doped glass presented in Table 1 and includes the $||U^{(t)}||^2$ matrix elements estimated by Carnall et al. [36] and evaluated by Kaminiskii [37].

The values of the three JO parameters were obtained by fitting the measured and computed line strengths of the absorption transitions using Equations (4) and (5). To calculate the Ω_t ($t = 2, 4, 6$) parameters for the PZLBPr sample under study, a least square fitting of values S_{exp} to S_{cal} was used.

When using all absorption transitions, it was found that the resulting Ω_2 parameter was negative, which from the definition is not acceptable. This controversial result is noticed in many compounds with Pr³⁺ ions [38–40].

Several methods have been proposed to resolve this problem, namely, the use of the modified JO theory [38,41]. The modified JO theory developed by Kornienko et al. [22,41–43] considers higher-order contributions in the forced electric dipole matrix elements; the resulting calculated line strength is provided using:

$$S_{\text{cal}} = \sum_{t=2,4,6} \Omega_t \left[1 + 2\alpha(E_J + E_{J'} - 2E_{4f}) \right] \times \left| \langle SLJ || U^{(t)} || S'L'J' \rangle \right|^2 \quad (6)$$

$E_{J'}$, E_J , and E_{4f} are the energies of the upper, lower states, and barycenter of the $4f$ configuration, respectively, the parameter α is used as a fitting parameter.

The Kornienko et al. [42] modified JO theory was used in this study with the value of the parameter α fixed to 10⁻⁵ cm as it is often estimated for Pr³⁺ glasses [22,43]. The procedure of the modified JO theory did not solve the problem and the Ω_2 value is still negative.

Another approach to overcoming this problem consists of excluding one of the absorption transitions from the fitting procedure [40,44–47]. For this Pr³⁺ sample, the exclusion of the ³H₄ → ³F₄ transition from the computation is investigated. Notably, absorptions due to transitions from the ground state up to ³F₄ and ³F₃ levels strongly overlap. In several studies, those two levels are combined into one: the (³F₄, ³F₃ → ³H₄) transition. Furthermore, a close observation of the absorption transition matrix elements of the Pr³⁺ ion shows that the Ω_2 parameter depends essentially on the ³H₄ → ³F₂ transition because of the high value of $\langle {}^3H_4 || U^{(2)} || {}^3F_2 \rangle$.

Without accounting for the ³H₄ → ³F₄ transition, the Ω_t numeric calculation produces an acceptable result. Table 2 presents JO parameters of Pr³⁺ in PZLBPr glass and Pr³⁺-

doped in other hosts. The calculated Judd–Ofelt parameters are in good agreement with literature values for Pr^{3+} -doped glasses [19,20,38,48]: similar trends ($\Omega_2 < \Omega_4 < \Omega_6$) have been found in PPbKANPr [19], TeO_2 - PbF_2 - AlF_3 - PrF_3 (TPA) [38], ASL [44], PTBPr [43], and $\text{Ca}_5(\text{PO}_4)_3\text{F}$ [48] glasses.

The acquired Ω_t values are utilized to obtain the rms deviation and recalculate the transition line strengths S_{cal} of the absorption bands using Equation (3). In our work, the rms deviation was determined to be $1.4868 \times 10^{-25} \text{ m}^2$. The significant mixing between the $4f$ and $5d$ orbitals may account for the increased rms difference between the estimated and observed oscillator strengths in the case of Pr^{3+} ions. The covalency, ionic composition, and symmetry of the RE ion's site are all factors connected to the Ω_2 parameter. In contrast, values Ω_4 and Ω_6 are closely connected to the basicity, hardness, and dielectric properties of the glass samples [19]. With an increase in the hardness of the host matrices' surroundings, Ω_6 decreases. In the present PZLBPr glass, the trend from $\Omega_2 < \Omega_4 < \Omega_6$ showed that there was more asymmetry and less covalency within the PrO group. The stimulated emission cross-section for the laser active medium is predicted by the spectroscopic quality factor $\chi = \Omega_4/\Omega_6$, which is found to be around 0.9 for this PZLBPr glass and similar to the value for the PPbKANPr0.5 sample [19].

Table 2. Comparison of the PZLBPr glass Judd–Ofelt parameters ($\Omega_t \times 10^{-20} \text{ cm}^2$) with those of other systems.

System	Ω_2	Ω_4	Ω_6	Trend	χ
PZLBPr [Present Work]:	0.018	1.641	1.816	$\Omega_2 < \Omega_4 < \Omega_6$	0.90
PPbKANPr0.5 [19]	1.51	18.03	19.81	$\Omega_2 < \Omega_4 < \Omega_6$	0.91
Phosphate [49]	4.19	4.29	6.40	$\Omega_2 < \Omega_4 < \Omega_6$	0.67
ZNBBP [50]	1.7	3.06	4.72	$\Omega_2 < \Omega_4 < \Omega_6$	0.64
BPGbPr [51]	0.70	2.96	7.03	$\Omega_2 < \Omega_4 < \Omega_6$	0.42
Oxyfluoride [52]	0.66	12.49	3.17	$\Omega_2 < \Omega_6 < \Omega_4$	3.94
$\text{Ca}_5(\text{PO}_4)_3\text{F}$ [48]	0.32	1.59	3.82	$\Omega_2 < \Omega_4 < \Omega_6$	0.41
LaF_3 [53]	0.12	1.77	4.78	$\Omega_2 < \Omega_4 < \Omega_6$	0.37
$\text{LiPrP}_4\text{O}_{12}$ [53]	1.82	2.83	6.54	$\Omega_2 < \Omega_4 < \Omega_6$	0.43
YAlO_3 [53]	2.00	6.00	7.00	$\Omega_2 < \Omega_4 < \Omega_6$	0.85
LiYF_4 [53]	0.00	8.07	7.32	$\Omega_2 < \Omega_6 < \Omega_4$	1.10
Oxy-Fluoride [21]	0.13	4.09	6.33	$\Omega_2 < \Omega_4 < \Omega_6$	0.64
TPA ($n = \text{cst}$) [38]	0.48	1.39	13.5	$\Omega_2 < \Omega_4 < \Omega_6$	0.10
TPA ($n \neq \text{cst}$) [38]	0.92	1.85	6.61	$\Omega_2 < \Omega_4 < \Omega_6$	0.27
TeO_2 - Li_2CO_3 - Pr_2O_3 [38]	3.81	5.81	4.1	$\Omega_2 < \Omega_6 < \Omega_4$	1.41
PTBPr [43]	3.07	3.36	8.68	$\Omega_2 < \Omega_6 < \Omega_4$	0.38

According to Table 2, the range of the spectroscopic quality factors for Pr^{3+} doped in various hosts is between 0.20 and 1.64.

For a change from a higher J' to a lower J -multiplet, the spontaneous emission probability $A_{J \rightarrow J'}$ is computed as follows:

$$A_{J \rightarrow J'} = \frac{1}{4\pi\epsilon_0} \frac{64\pi^4 e^2 v^3 n(n^2 + 2)^2}{27h(2J + 1)} S_{cal} \quad (7)$$

S_{cal} is the corresponding emission line strength calculated from Equation (6) using the value of Ω_t . In addition, the following formulas might be used to determine the radiative lifetime for electric dipole transitions between an excited state (J) and the lower-lying terminal manifolds (J'):

$$\tau = \frac{1}{\sum_{J'} A_{J \rightarrow J'}} \quad (8)$$

Over all final states (J'), the total of τ is calculated and the sum is taken over all final states J' .

The fluorescence branching ratio, β , is an important statistic for the laser designer since it describes the potential of achieving a stimulated emission from a certain transition and predicts the relative strength of lines from specified excited states.

$$\beta = A_{J \rightarrow J'} \cdot \tau \quad (9)$$

Table 3 shows the PZLBPr glass system's spectroscopic properties; ($A_{J \rightarrow J'}$), (τ), and (β) of excited states ${}^3\text{H}_4$, ${}^3\text{H}_5$, ${}^3\text{H}_6$, ${}^3\text{F}_2$, ${}^3\text{F}_3$, ${}^3\text{F}_4$, ${}^1\text{G}_4$, ${}^1\text{D}_2$, ${}^3\text{P}_0$, ${}^3\text{P}_1$, and ${}^3\text{P}_2$ of Pr^{3+} ions in the PZLBPr glasses.

It is observed that the lifetime trend decreases as ${}^3\text{H}_6 \gg {}^3\text{F}_2 > {}^3\text{F}_4 > {}^1\text{G}_4 > {}^3\text{F}_3 > {}^1\text{D}_2 > {}^3\text{P}_1 > {}^3\text{P}_0 \sim {}^3\text{P}_2$. There is a decreasing tendency of branching ratios for the emission transitions, ${}^3\text{F}_2 \rightarrow {}^3\text{H}_4 > {}^3\text{F}_3 \rightarrow {}^3\text{H}_4 > {}^3\text{F}_4 \rightarrow {}^3\text{H}_4 > {}^3\text{P}_0 \rightarrow {}^3\text{H}_4 > {}^1\text{G}_4 \rightarrow {}^3\text{H}_5 > {}^1\text{D}_2 \rightarrow {}^3\text{H}_4 > {}^3\text{P}_1 \rightarrow {}^3\text{H}_4 > {}^3\text{P}_2 \rightarrow {}^3\text{H}_4$. The branching ratios of ${}^3\text{P}_0 \rightarrow {}^3\text{H}_4$ (blue) and ${}^1\text{D}_2 \rightarrow {}^3\text{H}_4$ (red) transitions are estimated to be 67% and 47%, respectively. Thus, the blue and red/orange emissions are expected to be dominant among all visible transitions. An interesting result is that the branching ratio for the ${}^1\text{G}_4 \rightarrow {}^3\text{H}_5$ transition is larger than the ${}^1\text{G}_4 \rightarrow {}^3\text{H}_4$ transition. Precisely, ${}^1\text{G}_4 \rightarrow {}^3\text{H}_5$ presents an elevated fluorescence branching ratio ($\beta \sim 67\%$) characterizing the lasing potential of this transition, in the near-infrared region. Since the ${}^1\text{G}_4$ level has a sufficiently large energy gap with respect to the next lower level ${}^3\text{F}_4$, it emits via purely radiative relaxations an infrared fluorescence emission as shown in Figure 5. It should be noted that the ${}^1\text{G}_4$ level is efficiently pumpable at $1.01\ \mu\text{m}$, especially that high population inversion could be obtained, given that the excited initial state, (${}^3\text{H}_5$), relaxes directly to the ground state seeing the higher branching ratio of the ${}^3\text{H}_5 \rightarrow {}^3\text{H}_4$ transition.

The PL emission spectra of the prepared glass excited at 445 nm are shown in Figure 6. The ${}^3\text{P}_0 \rightarrow {}^3\text{H}_4$, ${}^3\text{P}_0 \rightarrow {}^3\text{H}_5$, ${}^1\text{D}_2 \rightarrow {}^3\text{H}_4$, ${}^3\text{P}_0 \rightarrow {}^3\text{H}_6$, and ${}^3\text{P}_0 \rightarrow {}^3\text{F}_2$ transitions of Pr^{3+} are responsible for the emission bands shown at 485, 525, 550, 600, and 640 nm, respectively. The type of glass host has a significant influence on the intensity of emission bands in the blue and reddish orange range. Two prominent transition peaks in the visible emission spectrum are attributed to ${}^3\text{P}_0 \rightarrow {}^3\text{H}_4$ (blue) and ${}^1\text{D}_2 \rightarrow {}^3\text{H}_4$ / ${}^3\text{P}_0 \rightarrow {}^3\text{H}_6$ (red/orange). The higher sub-levels of ${}^3\text{P}_0$ energy may be absorbed by a surrounding Pr^{3+} in the ground state when they are close together, which causes a decrease in the higher energy levels of ${}^3\text{P}_0$. The spectrum of ${}^3\text{P}_0 \leftrightarrow {}^3\text{H}_4$ overlaps the high-energy emission and low-energy absorption sides.

Furthermore, compared to the ${}^3\text{P}_0 \rightarrow {}^3\text{H}_4$ transition, the emission intensity increase from the ${}^1\text{D}_2$ state is significantly lower. Because of the population or depopulation of the ${}^1\text{D}_2$ state of Pr^{3+} ions in host glasses is significantly influenced by multi-phonon relaxation and cross relaxation. Pr^{3+} ions undergo the ${}^3\text{P}_0 \rightarrow {}^3\text{H}_4$ transition as the excitation energy is changed from the lower ${}^3\text{P}_0$ state to the ${}^1\text{D}_2$ state, resulting in reddish orange luminescence. Under 445 nm excitation, Bo Zhou et al. [5] examined the visible PL spectra of Pr^{3+} doped fluorotellurite glasses. They determined that the emission bands at wavelengths of 490, 528, 611, and 643 nm, respectively, correspond to the Pr^{3+} transitions of (${}^3\text{P}_1$, ${}^3\text{P}_0$) $\rightarrow {}^3\text{H}_4$, ${}^3\text{P}_0 \rightarrow {}^3\text{H}_5$, (${}^3\text{P}_1$, ${}^3\text{P}_0$) $\rightarrow {}^3\text{H}_6$, and ${}^3\text{P}_0 \rightarrow {}^3\text{F}_2$, respectively. Our data are excellent agreement with those of other glasses described in Refs. [5,54–56]. As a consequence, we can conclude that PZLBPr is a high phonon glass that can occupy the energy gap between the visible range ${}^3\text{P}_0$ and ${}^1\text{D}_2$ states of Pr^{3+} ions and the red/orange emission caused by ${}^1\text{D}_2 \rightarrow {}^3\text{H}_4$.

Figure 7 displays the NIR luminescence emission spectra of PZLBPr-produced glass excited by 445 nm (${}^3\text{P}_2$) at wavelengths between 850 and 1700 nm. Observing that the (${}^1\text{D}_2 \rightarrow {}^3\text{F}_3$, ${}^3\text{F}_4$) and (${}^1\text{G}_4 \rightarrow {}^3\text{H}_5$) and (${}^1\text{G}_4 \rightarrow {}^3\text{H}_5$) transitions of Pr^{3+} are responsible for the near-infrared luminescence bands at 1030 and 1350 nm is significant for optical fiber amplifiers operating in the second telecommunication window [53,55,56]. The ${}^1\text{D}_2 \rightarrow {}^1\text{G}_4$ transition of Pr^{3+} is responsible for the strong NIR luminescence band with a center wavelength of around 1460 nm. The ultra-broadband near-infrared fluorescence band ${}^3\text{F}_3$, ${}^3\text{F}_4 \rightarrow {}^3\text{H}_4$ transition at around 1685 nm also contributed. As can be seen in Figure 7, the full-width at half-maximum

(FWHM) for the equivalent $^1D_2 \rightarrow ^1G_4$ transition emission is 156nm, which indicates that the PZLBPr glass is very suitable for broadband amplification of E-, S-, C-, and L-bands.

Table 3. The spectroscopic parameters of the PZLBPr glass system.

Transition	Wavelength (nm)	A (s^{-1})	τ (ms)	β (%)	
$^3P_2 \rightarrow$	3H_4	431.77	4393.6	0.040	17.6
	3H_5	476.0	5891.9		23.7
	3H_6	532.72	7053.9		28.3
	3F_2	550.54	3420.7		13.7
	3F_3	597.18	2776.2		11.1
	3F_4	613.28	1078.3		4.3
	1G_4	755.32	268.29		1.1
	1D_2	1716.4	26.99		0.1
	3P_0	5647.2	0.023		0.0
3P_1	8671.9	0.013		0.0	
$^3P_1 \rightarrow$	3H_4	454.39	5762.6	0.076	43.9
	3H_5	503.64	0		0.0
	3H_6	567.59	1391.1		10.6
	3F_2	587.86	47.37		0.4
	3F_3	641.35	2435.6		18.6
	3F_4	659.95	3141.5		24.0
	1G_4	827.39	338.42		2.6
	1D_2	2139.9	0.2739		0.0
	3P_0	16190	0		0.0
$^3P_0 \rightarrow$	3H_4	467.51	16068	0.041	67.4
	3H_5	519.81	150.98		0.6
	3H_6	588.21	3329.6		14.0
	3F_2	610.01	139.41		0.6
	3F_3	667.80	0.00		0.0
	3F_4	687.99	3539.2		14.8
	1G_4	871.95	609.13		2.6
	1D_2	2465.8	0.10		0.0
$^1D_2 \rightarrow$	3H_4	576.89	737.95	0.147	47.8
	3H_5	658.66	14.84		1.0
	3H_6	772.48	294.00		19.1
	3F_2	810.52	291.04		18.9
	3F_3	915.82	42.40		2.7
	3F_4	954.23	49.17		3.2
	1G_4	1349.0	113.84		7.4
$^1G_4 \rightarrow$	3H_4	1007.9	18.33	3.096	5.7
	3H_5	1287.1	218.72		67.7
	3H_6	1807.6	71.32		22.1
	3F_2	2030.6	2.19		0.7
	3F_3	2852.3	2.42		0.7
	3F_4	3261.1	9.96		3.1
$^3F_4 \rightarrow$	3H_4	1458.8	199.48	4.995	99.7
	3H_5	2126.5	0.00		0.0
	3H_6	4055.7	0.00		0.0
	3F_2	5381.7	0.69		0.3
	3F_3	22,753.0	0.01		0.0
$^3F_3 \rightarrow$	3H_4	1558.8	401.43	2.489	99.9
	3H_5	2345.7	0.00		0.0
	3H_6	4935.5	0.00		0.0
	3F_2	7049.1	0.20		0.01
$^3F_2 \rightarrow$	3H_4	2001.4	127.81	7.823	100
	3H_5	3515.5	0.00		0.0
	3H_6	16,460.0	0.00		0.0
$^3H_6 \rightarrow$	3H_4	2278.4	11.59	86.286	100
	3H_5	4470.3	0.00		0.0
$^3H_5 \rightarrow$	3H_4	4646.6	0.00		0.0

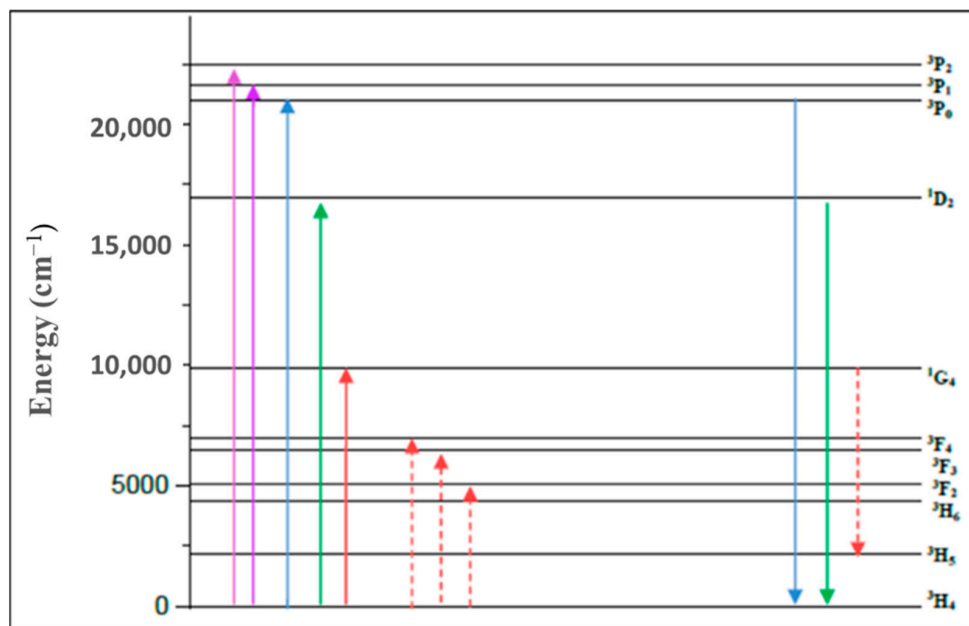


Figure 5. Energy level diagram of Pr³⁺ ions.

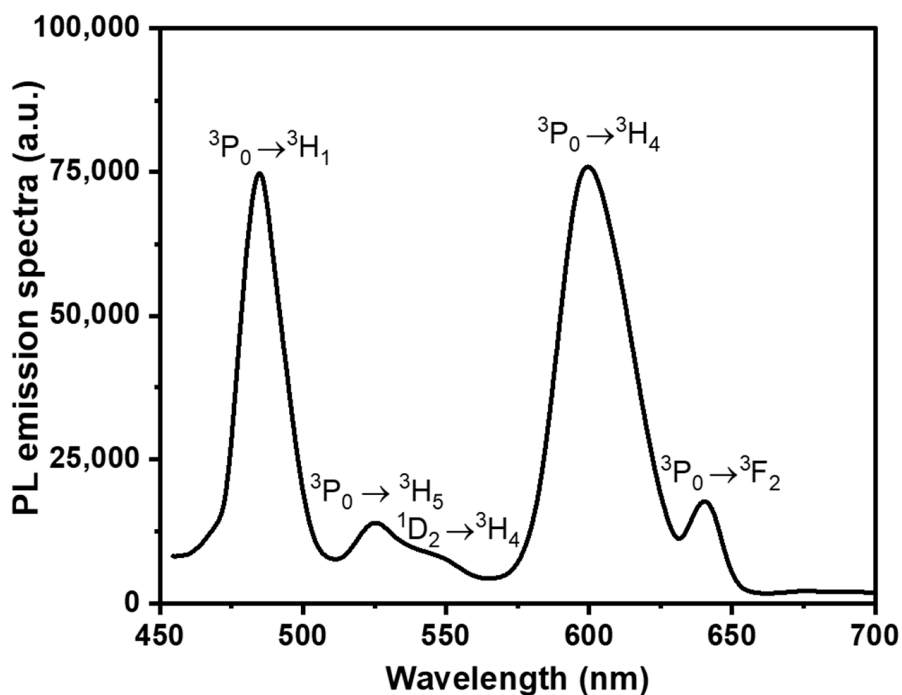


Figure 6. VIS PL emission spectra of PZLBPr under excitation 445 nm.

According to X. Liu et al. [1], the associated ¹D₂ → ¹G₄ transition emission has a 140 nm full-width at half-maximum (FWHM), which enables Pr³⁺-doped NZPPT glasses attractive for broadband amplification covering the entire E-, S-, C-, and L-bands. The ultra-broadband emission at 1.48 μm has a peak in intensity at 1476 nm. Additionally, previous findings in [1,2,57,58] suggest that Pr³⁺-doped borate, phosphate, and silicate glass fiber amplifiers operating in the fifth optical communications window may be useful (1380–1525 nm): the PZLBPr glass is a better choice for usage in optical communication devices as it has a greater FWHM of the transition emission of ¹D₂ → ¹G₄ (156 nm) than the present glass does.

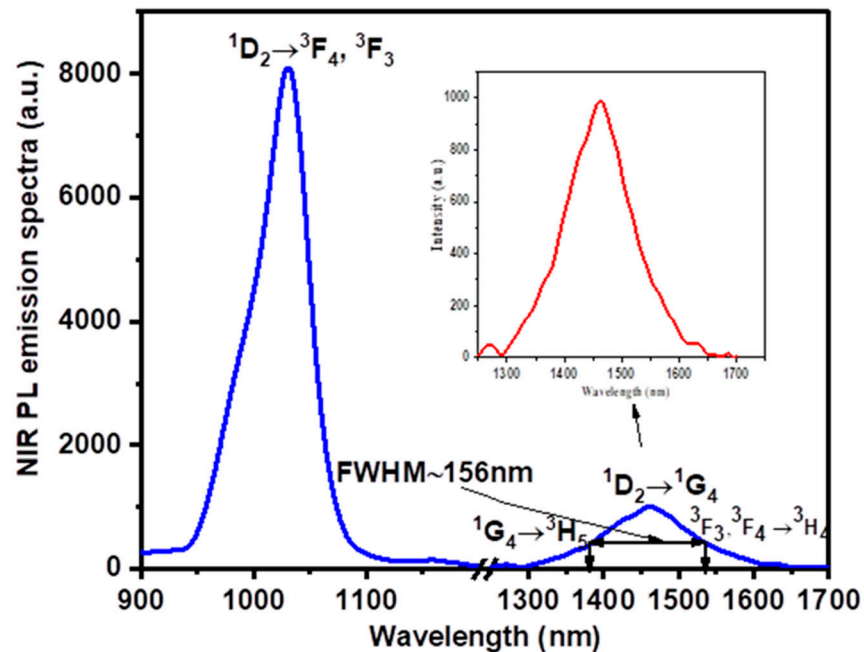


Figure 7. NIR PL emission spectra of PZLBPr under excitation at 445 nm.

The lifetime values are calculated using the formula: $\tau_{exp} = \int t\varepsilon(t)/\varepsilon(t)$, where the decay curve is dependent on time, as shown in [14,17]. Figure 8 depicts the PL decay of stimulated levels. The radiative lifetime, estimated to be 147.1 μs , and the experimental lifetime, estimated to be 128.4 μs by fitting the fluorescence decay curve, are used to calculate the quantum efficiency, $\eta_{eff} = \frac{\tau_{exp}}{\tau_{rad}}$, for a luminescence level of 1D_2 to 1G_4 . The near-infrared emission from the 1D_2 level is efficient for creating optical signal amplification in a specific optical communications band, as shown by the quantum efficiency of the Pr^{3+} : 1D_2 level, which is equivalent to 87.3%. Together, these findings demonstrate that PZBLPr glass's specific optical communications band may effectively produce optical signal amplification via the near-infrared emission at the 1D_2 level.

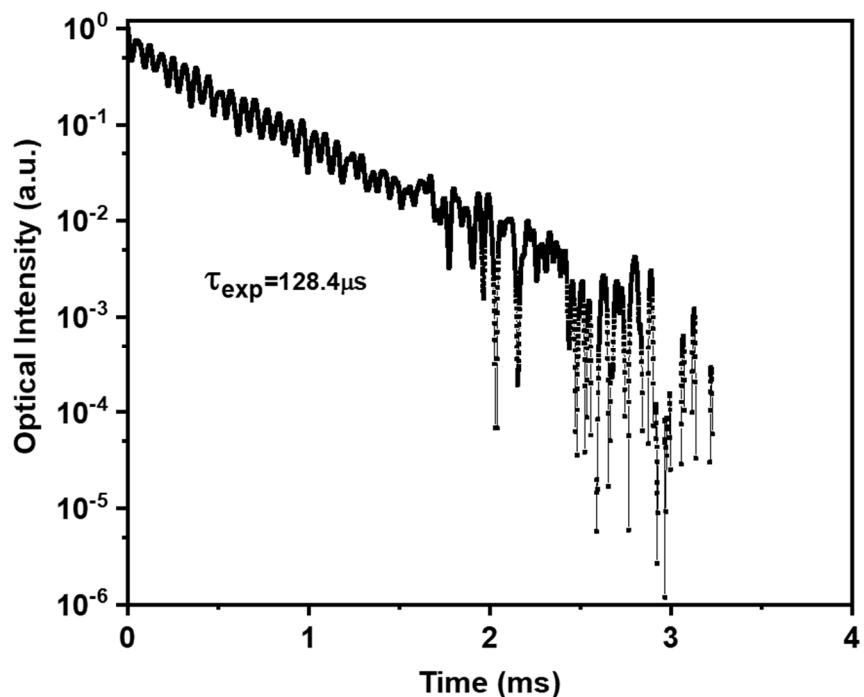


Figure 8. The Pr^{3+} : 1D_2 fluorescence decay level of PZLBPr under excitation at 445 nm.

4. Conclusions

The incorporation of halide ions (F^- and Cl^-) with Pr^{3+} ions into the present phosphate matrix leads to improvement of the high value of the optical energy gap compared to some phosphate glasses reported previously. The valuation of Judd–Ofelt parameters of PZBLPr glasses achieved the following: ($\Omega_2 = 0.0181 \times 10^{-20} \text{ cm}^2$, $\Omega_4 = 1.641 \times 10^{-20} \text{ cm}^2$, $\Omega_6 = 1.816 \times 10^{-20} \text{ cm}^2$). The trend of $\Omega_2 < \Omega_4 < \Omega_6$ that occurred in the studied glasses indicated higher asymmetry and lower covalency between Pr–O groups. In addition, the halide ions led to a decrease in the covalency otherwise an increase in the ionicity of the structure of PZBLPr glasses. The large quantum efficiency of $Pr^{3+}:^1D_2$ (=87.3%) with full-width at half maximum of 156 nm was reported in PZLBPr glass. Therefore, based on this analysis, it can be concluded that PZLBPr glass has potential for broadband near-IR functioning and can have its communications transmission window increased at 445 nm.

Author Contributions: B.C.: Conceptualization, methodology, investigation, writing—original draft, writing—review and editing; K.D.: Conceptualization, methodology, formal analysis, investigation, writing—original draft; R.M.: Methodology, writing—review and editing, visualization; M.S.A.: Formal analysis, investigation, writing—original draft, writing—review and editing, visualization; K.I.H.: Methodology, formal analysis, writing—review and editing, visualization; A.M.A.: Formal analysis, review and editing, visualization; A.M.H.: Formal analysis, visualization, writing—review and editing; B.B.-G.: Formal analysis, visualization, writing—review and editing; M.R.: Methodology, formal analysis, writing—review and editing, visualization; E.S.Y.: Conceptualization, methodology, investigation, funding acquisition, writing—review and editing, visualization. All authors have read and agreed to the published version of the manuscript.

Funding: This research was funded by the Deputyship for Research and Innovation, Ministry of Education, Saudi Arabia, grant number IFP-KKU-2020/7.

Institutional Review Board Statement: Not applicable.

Informed Consent Statement: The authors declare that they have no known competing financial interests or personal relationships that could have appeared to influence the work reported in this paper.

Data Availability Statement: Not applicable.

Acknowledgments: The authors extend their appreciation to the Deputyship for Research and Innovation, Ministry of Education, Saudi Arabia, for funding this research work through project number IFP-KKU-2020/7.

Conflicts of Interest: The authors declare no conflict of interest.

References

1. Liu, X.; Chen, B.J.; Pun, E.Y.B.; Lin, H. Ultra-broadband near-infrared emission in praseodymium ion doped germanium tellurite glasses for optical fiber amplifier at E-, S-, C-, and L-band. *J. Appl. Phys.* **2012**, *111*, 116101. [[CrossRef](#)]
2. Zhou, B.; Pun, E.Y.-B. Superbroadband near-IR emission from praseodymium-doped bismuth gallate glasses. *Opt. Lett.* **2011**, *36*, 2958–2960. [[CrossRef](#)] [[PubMed](#)]
3. Damak, K.; Yousef, E.; AlFaify, S.; Rüssel, C.; Maalej, R. Raman, green and infrared emission cross-sections of Er^{3+} doped TZPPN tellurite glass. *Opt. Mater. Express* **2014**, *4*, 597. [[CrossRef](#)]
4. Damak, K.; Yousef, E.S.; Al-Shihri, A.S.; Seo, H.J.; Rüssel, C.; Maalej, R. Quantifying Raman and emission gain coefficients of Ho^{3+} doped $TeO_2 \cdot ZnO \cdot PbO \cdot PbF_2 \cdot Na_2O$ (TZPPN) tellurite glass. *Solid State Sci.* **2014**, *28*, 74–80. [[CrossRef](#)]
5. Zhou, B.; Tao, L.; Tsang, Y.H.; Jin, W.; Pun, E. Superbroadband near-IR photoluminescence from Pr^{3+} -doped fluorotellurite glasses. *Opt. Express* **2012**, *20*, 3803–3813. [[CrossRef](#)]
6. Shen, L.; Chen, B.; Lin, H.; Pun, E. Praseodymium ion doped phosphate glasses for integrated broadband ion-exchanged waveguide amplifier. *J. Alloys Compd.* **2015**, *622*, 1093–1097. [[CrossRef](#)]
7. Sheng, Q.; Wang, X.; Chen, D. Near-infrared emission from Pr-doped borophosphate glass for broadband telecommunication. *J. Lumin.* **2013**, *135*, 38–41. [[CrossRef](#)]
8. Han, X.; Shen, L.; Pun, E.Y.B.; Ma, T.; Lin, H. Pr^{3+} -doped phosphate glasses for fiber amplifiers operating at 1.38–1.53 μm of the fifth optical telecommunication window. *Opt. Mater.* **2014**, *36*, 1203–1208. [[CrossRef](#)]
9. Belançon, M.P.; Marconi, J.D.; Ando, M.F.; Barbosa, L.C. Near-IR emission in Pr^{3+} single doped and tunable near-IR emission in Pr^{3+}/Yb^{3+} codoped tellurite tungstate glasses for broadband optical amplifiers. *Opt. Mater.* **2014**, *36*, 1020–1026. [[CrossRef](#)]

10. Nachimuthu, P.; Vithal, M.; Jagannathan, R. Absorption and Emission Spectral Properties of Pr³⁺, Nd³⁺, and Eu³⁺ Ions in Heavy-Metal Oxide Glasses. *J. Am. Ceram. Soc.* **2004**, *83*, 597–604. [CrossRef]
11. Balda, R.; Fernández, J.; De Pablos, A.; Fdez-Navarro, J.M. Spectroscopic properties of Pr³⁺ ions in lead germanate glass. *J. Phys. Condens. Matter* **1999**, *11*, 7411–7421. [CrossRef]
12. Jacinto, C.; Oliveira, S.L.; Nunes, L.A.O.; Myers, J.D.; Myers, M.J.; Catunda, T. Normalized-lifetime thermal-lens method for the determination of luminescence quantum efficiency and thermo-optical coefficients: Application to Nd³⁺-doped glasses. *Phys. Rev. B* **2006**, *73*, 125107. [CrossRef]
13. Righini, G.; Ferrari, M. Photoluminescence of rare-earth-doped glasses. *Riv. Nuovo Cim.* **2006**, *28*, 1–53. [CrossRef]
14. Burtan-Gwizdala, B.; Reben, M.; Cisowski, J.; Yousef, E.S.; Lisiecki, R.; Nosidlak, N. Strong emission at 1000 nm from Pr³⁺/Yb³⁺-codoped multicomponent tellurite glass. *Pure Appl. Chem.* **2021**, *94*, 147–156. [CrossRef]
15. Li, Y.; Yu, Q.; Huang, L.; Wang, J.; Su, Q. Near ultraviolet and visible-to-near-infrared spectral converting properties and energy transfer mechanism of Sr₂SiO₄:Ce³⁺, Pr³⁺ phosphor. *Opt. Mater. Express* **2014**, *4*, 227. [CrossRef]
16. Mahlke, G.; Gössing, P. *Corning Cable Systems; Fiber Optic Cables*; Publicis MCD Corporate Publishin: Munich, Germany, 2001; pp. 13–30.
17. Burtan-Gwizdala, B.; Reben, M.; Cisowski, J.; Lisiecki, R.; Ryba-Romanowski, W.; Jarzabek, B.; Mazurek, Z.; Nosidlak, N.; Grelowska, I. The influence of Pr³⁺ content on luminescence and optical behavior of TeO₂-WO₃-PbO-Lu₂O₃ glass. *Opt. Mat.* **2015**, *47*, 231–236. [CrossRef]
18. Seshadri, M.; Bell, M.J.V.; Anjos, V.; Messaddeq, Y. Spectroscopic investigations on Yb³⁺ doped and Pr³⁺/Yb³⁺ co-doped tellurite glasses for photonic applications. *J. Rare Earths* **2021**, *39*, 33–42. [CrossRef]
19. Basavapoornima, C.; Kesavulu, C.; Maheswari, T.; Pecharapa, W.; Depuru, S.R.; Jayasankar, C. Spectral characteristics of Pr³⁺-doped lead based phosphate glasses for optical display device applications. *J. Lumin.* **2020**, *228*, 117585. [CrossRef]
20. Sangwaranatee, N.W.; Kiwsakunkran, N.; Kaewkhao, J. Investigation on Physical and Optical of Praseodymium Doped Sodium Aluminum Barium Phosphate Glasses. *J. Phys. Conf. Ser.* **2020**, *1428*, 12031. [CrossRef]
21. Ritu, S.; Rao, A.S.; Deopa, N.; Venkateswarlu, M.; Jayasimhadri, M.; Haranath, D.; Vijaya Prakash, G. Spectroscopic study of Pr³⁺ ions doped Zinc Lead Tungsten, Tellurite glasses for visible photonic device applications. *Opt. Mater.* **2018**, *78*, 457e464.
22. Flizikowski, G.A.S.; Zanuto, V.S.; Nunes, L.A.O.; Baesso, M.L.; Malacarne, L.C.; Astrath, N.G.C. Standard and modified Judd-Ofelt theories in Pr³⁺-doped calcium, aluminosilicate glasses: A comparative analysis. *J. Alloys Compd.* **2018**, *780*, 705–710. [CrossRef]
23. Davis, E.A.; Mott, N.F. Conduction in non-crystalline systems V. Conductivity, optical absorption and photoconductivity in amorphous semiconductors. *Philos. Mag.* **1970**, *22*, 903–922. [CrossRef]
24. Afef, B.; Hegazy, H.H.; Algarni, H.; Yang, Y.; Damak, K.; Yousef, E.; Maalej, R. Spectroscopic analysis of trivalent Nd³⁺/Yb³⁺ ions co-doped in PZS host glasses as a new laser material at 1.06 μm. *J. Rare Earths* **2017**, *35*, 361–367. [CrossRef]
25. Afef, B.; Alqahtani, M.M.; Hegazy, H.H.; Yousef, E.; Damak, K.; Maalej, R. Green and near-infrared emission of Er³⁺ doped PZS and PZC glasses. *J. Lumin.* **2018**, *194*, 706–712. [CrossRef]
26. Hussein, K.I.; Alqahtani, M.S.; Alzahrani, K.J.; Alqahtani, F.F.; Zahran, H.Y.; Alshehri, A.M.; Yahia, I.S.; Reben, M.; Yousef, E.S. The Effect of ZnO, MgO, TiO₂, and Na₂O Modifiers on the Physical, Optical, and Radiation Shielding Properties of a TeTaNb Glass System. *Materials* **2022**, *15*, 1844. [CrossRef] [PubMed]
27. Charfi, B.; Damak, K.; Alqahtani, M.S.; Hussein, K.I.; Alshehri, A.M.; Elkhoshkhany, N.; Assiri, A.L.; Alshehri, K.F.; Reben, M.; Yousef, E.S. Luminescence and Gamma Spectroscopy of Phosphate Glass Doped with Nd³⁺/Yb³⁺ and Their Multifunctional Applications. *Photonics* **2022**, *9*, 406. [CrossRef]
28. Rayan, D.A.; Elbashar, Y.H.; Rashad, M.M.; El-Korashy, A. Optical spectroscopic analysis of cupric oxide doped barium phosphate glass for bandpass absorption filter. *J. Non-Cryst. Solids* **2013**, *382*, 52–56. [CrossRef]
29. Ghauri, M.; Siddiqi, S.; Shah, W.; Ashiq, M.; Iqbal, M. Optical properties of zinc molybdenum phosphate glasses. *J. Non-Cryst. Solids* **2009**, *355*, 2466–2471. [CrossRef]
30. Elbashar, Y.H. Structural and spectroscopic analyses of copper doped P₂O₅-ZnO-K₂O-Bi₂O₃ glasses. *Process Appl. Ceram.* **2015**, *9*, 169–173. [CrossRef]
31. Judd, B.R. Optical Absorption Intensities of Rare-Earth Ions. *Phys. Rev.* **1962**, *127*, 750–761. [CrossRef]
32. Ofelt, G.S. Intensities of crystal spectra of rare-earth ions. *J. Chem. Phys.* **1962**, *37*, 511–520. [CrossRef]
33. Damak, K.; Maalej, R.; Yousef, E.S.; Qusti, A.H.; Rüssel, C. Thermal and spectroscopic properties of Tm³⁺ doped TZPPN transparent glass laser material. *J. Non-Cryst. Solids* **2012**, *358*, 2974–2980. [CrossRef]
34. Sharma, Y.K.; Singh, R.K.; Pal, S. Praseodymium Ion Doped Sodium Borosilicate Glasses: Energy Interaction and Radiative Properties. *Am. J. Condens. Matter Phys.* **2015**, *5*, 10–18. [CrossRef]
35. Jia, G.; Wang, H.; Lu, X.; You, Z.; Li, J.; Zhu, Z.; Tu, C. Optical properties of Pr³⁺-doped SrWO₄ crystal. *Appl. Phys. A* **2007**, *90*, 497–502. [CrossRef]
36. Carnall, W.T.; Crosswhite, H.; Crosswhite, H.M. Energy Level Structure and Transition Probabilities in the Spectra of the Trivalent Lanthanides in LaF₃. United States: N. p.; Technical Report 1978; TRN: 79-005910. Available online: <https://www.osti.gov/biblio/6417825/> (accessed on 4 August 2022). [CrossRef]
37. Kaminskii, A.A. *Laser Crystals: Their Physics and Properties*; Springer: Berlin, Germany, 1981; pp. 157–158.
38. Lalla, E.A.; Konstantinidis, M.; De Souza, I.; Daly, M.G.; Martín, I.R.; Lavín, V.; Rodríguez-Mendoza, U.R. Judd-Ofelt parameters of RE³⁺-doped fluorotellurite glass, (RE³⁺: Pr³⁺, Nd³⁺, Sm³⁺, Tb³⁺, Dy³⁺, Ho³⁺, Er³⁺, and Tm³⁺). *J. Alloys Compd.* **2020**, *845*, 156028. [CrossRef]

39. Ajithkumar, G.; Gupta, P.K.; Gin Jose, N.V. Unnikrishnan Judd–Ofelt intensity parameters and laser analysis of Pr³⁺-doped phosphate glasses sensitized by Mn²⁺ Ions. *J. Non-Cryst. Solids* **2000**, *275*, 93–106. [[CrossRef](#)]
40. Malta, O.; Carlos, L. Intensities of 4f–4f transitions in glass materials. *Quim. Nova* **2003**, *26*, 889–895. [[CrossRef](#)]
41. Goldner, P.; Auzel, F. Application of standard and modified Judd–Ofelt theories to a praseodymium-doped fluorozirconate glass. *J. Appl. Phys.* **1996**, *79*, 7972. [[CrossRef](#)]
42. Kornienko, A.A.; Kaminskii, A.A.; Dunina, E.B. Dependence of the Line Strength of f–f Transitions on the Manifold Energy. II. Analysis of Pr³⁺ in KPrP4O12. *Phys. Status Solidi* **1990**, *157*, 267–273. [[CrossRef](#)]
43. Kumar, M.V.V.; Rama Gopal, K.; Reddy, R.R.; Lokeswara Reddy, G.V.; Sooraj Hussain, N.; Jamalaihah, B.C. Application of modified Judd–Ofelt theory and the evaluation of radiative properties of Pr³⁺-doped lead telluroborate glasses for laser applications. *J. Non-Cryst. Solids* **2013**, *364*, 20–27. [[CrossRef](#)]
44. Sattayaporn, S.; Loiseau, P.; Aka, G.; Klimin, S.; Boldyrev, K.; Mavrin, B. Fine spectroscopy and Judd–Ofelt analysis of Pr³⁺-doped Sr_{0.7}La_{0.3}Mg_{0.3}Al_{11.7}O₁₉ (Pr:ASL). *J. Lumin.* **2019**, *219*, 116895. [[CrossRef](#)]
45. Guo, W.; Lin, Y.; Gong, X.; Chen, Y.; Luo, Z.; Huang, Y. Growth and spectroscopic properties of Pr³⁺:NaLa(MoO₄)₂ crystal. *J. Appl. Phys.* **2008**, *104*, 53105. [[CrossRef](#)]
46. Génova, R.T.; Martin, I.R.; Rodriguez-Mendoza, U.R.; Lahoz, F.; Lozano-Gorrin, A.D.; Nunez, P.; Gonzalez-Platas, J.; Lavin, V. Optical intensities of Pr³⁺ ions in transparent oxyfluoride glass and glass–ceramic. Applications of the standard and modified Judd–Ofelt theories. *J. Alloys Compd.* **2004**, *380*, 167–172. [[CrossRef](#)]
47. Sojka, L.; Tang, Z.; Furniss, D.; Sakt, H.; Oladeji, A.; Beres-Pawlik, E.; Dantanarayana, H.; Faber, E.; Seddon, A.B.; Benson, T.M.; et al. Broadband, mid-infrared emission from Pr³⁺-doped GeAsGaSe chalcogenide fiber, optically clad. *Opt. Mater.* **2014**, *36*, 1076–1082. [[CrossRef](#)]
48. Sardar, D.K.; Russell, C.C., III. Optical transitions, absorption intensities, and intermanifold emission cross sections of Pr³⁺(4f₂) in Ca₅(PO₄)₃F crystal host. *Appl. Phys.* **2004**, *95*, 10. [[CrossRef](#)]
49. Mazurak, Z.; Bodyl, S.; Lisiecki, R.; Gabrys-Pisarska, J.; Czaja, M. Optical properties of Pr³⁺, Sm³⁺ and W³⁺-doped P₂O₅–CaO–SrO–BaO phosphate glass. *Opt. Mater.* **2010**, *32*, 547–553. [[CrossRef](#)]
50. Hegde, V.; Dwaraka Viswanath, C.S.; Chauhan, N.; Mahato, K.K.; Kamath, S.D. Photoluminescence and thermally stimulated luminescence properties of Pr³⁺-doped zinc sodium bismuth borate glasses. *Opt. Mater.* **2018**, *84*, 268–277. [[CrossRef](#)]
51. Herrera, A.; Jacinto, C.; Becerra, A.R.; Franzen, P.L.; Balzaretto, N.M. Multichannel emission from Pr³⁺-doped heavy-metal oxide glass B₂O₃–PbO–GeO₂–Bi₂O₃ for broadband signal amplification. *J. Lumin.* **2016**, *180*, 341–347. [[CrossRef](#)]
52. Klimesz, B.; Dominiak-Dzik, G.; Zelechower, M.; Ryba-Romanowski, W.J. Optical study of GeO₂-PbO-PbF₂ oxyfluoride glass singly doped with Pr³⁺, Nd³⁺, Sm³⁺ and Eu³⁺. *J. Alloys Compd.* **2005**, *403*, 76–85. [[CrossRef](#)]
53. Kaminskii, A.A. *Crystalline Lasers: Physical Processes and Operating Schemes*; CRC Press: New York, NY, USA, 1996; 296p.
54. Oliveira, A.S.; Gouveia, E.A.; De Araujo, M.T.; Gouveia-Neto, A.S.; De Araujo, C.B.; Messaddeq, Y. Twentyfold blue upcon-version emission enhancement through thermal effects in Pr³⁺/Yb³⁺-co-doped fluorindate glasses excited at 1.064 μm. *J. Appl. Phys.* **2000**, *87*, 4274–4278. [[CrossRef](#)]
55. Shojiya, M.; Kawamoto, Y.; Kadono, K. Judd–Ofelt parameters and multiphonon relaxation of Ho³⁺ ions in ZnCl₂-based glass. *J. Appl. Phys.* **2001**, *89*, 4944–4950. [[CrossRef](#)]
56. Naresh, V.; Ham, B.S. Influence of multiphonon and cross relaxations on 3P₀ and 1D₂ emission levels of Pr³⁺-doped borosilicate glasses for broad band signal amplification. *J. Alloys Compd.* **2016**, *664*, 321–330. [[CrossRef](#)]
57. Lei, W.H.; Chen, B.J.; Zhang, X.L.; Pun, E.Y.B.; Lin, H. Optical evaluation on Nd(3+)-doped phosphate glasses for O-band amplification. *Appl. Opt.* **2011**, *50*, 835–841. [[CrossRef](#)] [[PubMed](#)]
58. Zhou, D.C.; Wang, R.F.; Yang, Z.W.; Song, Z.G.; Yin, Z.Y.; Qiu, J.B. Spectroscopic properties of Tm³⁺-doped TeO₂-R₂O-La₂O₃ glasses for 1.47 μm optical amplifiers. *J. Non-Cryst. Solids* **2011**, *357*, 2409–2412. [[CrossRef](#)]